ELSEVIER

Chemical Engineering Science 61 (2006) 3362–3378

Chemical Engineering Science

www.elsevier.com/locate/ces

Simultaneous process and control system design for grade transition in styrene polymerization

Mariano Asteasuain, Alberto Bandoni, Claudia Sarmoria, Adriana Brandolin*

Planta Piloto de Ingeniería Química (UNS - CONICET), CC 717, (8000) Bahía Blanca, Argentina

Received 24 May 2005; received in revised form 21 November 2005; accepted 5 December 2005
Available online 3 February 2006

Abstract

We present a comprehensive approach to the simultaneous design and control of a continuous stirred tank reactor (CSTR) for styrene solution polymerization that must be able to produce different polymer grades. The resulting tool allows simultaneous selection of the polymerization equipment, the multivariable feedforward–feedback controller's structure and tuning parameters, the steady states and the transition paths between them. For this purpose a multiobjective optimization is implemented to minimize the annualized reactor cost, the operating costs, the production of off-specification polymer and the transition time between steady states. Trade-offs between the sometimes conflicting objectives are dealt with by the optimization. Unlike many previous grade transition studies, steady states are not known a priori. The only known parameters are the target molecular weights to be produced at each steady state. We have analyzed three different scenarios, and propose practical criteria for selecting the most reasonable optimum when the solution is not unique.

Keywords: Process control; Polymerization; Mixed-integer; Dynamic optimization; Simultaneous design and control; Chemical processes

1. Introduction

Polymer manufacture is one of the most important industries worldwide, and is constantly growing in sales volume. It has been estimated that polymer consumption in developed and developing countries increases in proportion to their gross national products. Nowadays, the volume of synthetic polymers produced is greater than that of steel (Stepto et al., 2003). However, higher energy costs, more stringent environmental regulations, increased worldwide competition and the demand for lower prices have required more efficiency from production processes, and therefore a strong need to improve plant design and process operability has appeared.

Usually, designs of chemical processes are based on the optimization of objective functions that measure the economics of steady-state operating points. Intense research has been performed on steady-state optimization of polymerization processes. For instance, Brandolin et al. (1991) and Asteasuain et al. (2001) studied a high-pressure ethylene polymerization reactor. They analyzed the steady-state profiles of temperature and initiator concentration, and different reactor configurations. They aimed at maximizing conversion and minimizing cooling costs, while keeping product quality within specified values. Ray and Gupta (1985, 1986) and Srivastava and Gupta (1991) studied the steady-state optimization of nylon 6 tubular reactors. Their optimization variable was the jacket temperature, but they also analyzed sensitivity to other parameters, such as the reactor length and the desired average molecular weight. McKenna and Malone (1990) and McKenna (1996) developed a procedure for the systematic design of polymer production processes. Based on the work by Douglas (1985), they presented a combination of heuristics and design estimates specific for polymerization processes, which allow to choose among alternatives and to identify the most promising designs. A sensitivity evaluation allowed them to identify critical parameters of the design. This conceptual design procedure was applied to different homo- and co-polymerization processes. Costa Jr. et al. (2003) optimized the steady-state operation of a three-zone tubular styrene polymerization reactor. Considering the wall temperature of each reactor zone as the only manipulated variable, they solved a multiobjective optimization in order to

* Corresponding author. Tel.: +54 291 486 1700; fax: +54 291 486 1600.
E-mail address: abrandolin@plapiqui.edu.ar (A. Brandolin).

0009-2509/$ - see front matter © 2006 Elsevier Ltd. All rights reserved.
doi:10.1016/j.ces.2005.12.012

find maximum conversion with minimum polydispersity. They obtained optimal operating conditions that yielded lower polydispersity at the same conversion level than when uniform temperature existed along the whole reactor wall. Nascimento et al. (2000) used a neural network based approach for the optimization of the nylon-6,6 polymerization in a twin-screw extruder reactor. With the neural network, they mapped a grid of more than 10^5 points of the input variables, and afterwards they screened this grid first for feasible points and then for qualitative economic optimums.

In the polymer industry, profitability depends not only on steady-state operation, but also on grade transition policies. Usually, several polymer grades are produced with the same equipment in continuous plants. Market demands motivate periodic changes from one grade to another, so optimal grade transition operation (minimization of off-specification product and transition time) is an essential feature of a lucrative process. For this reason, much work has been devoted to grade transition optimization. McAuley and MacGregor (1992) developed optimal transition policies among three polyethylene grades in a gas-phase reactor. Using dynamic optimization they calculated the best profiles of the input variables. Takeda and Ray (1999) studied the grade transition optimization in polyolefin loop reactors, comparing results with and without constraints in the state variables. Cervantes et al. (2002) analyzed grade transitions in a low-density polyethylene plant. They calculated optimal profiles of butane feed and purge streams in order to minimize transition time. In these works, however, grade transitions were conducted between fully specified steady states. This is the approach that has been most commonly used, where it is assumed that the steady states have been previously determined according to some criteria, for instance, steady-state optimization. Some works dealt both with the optimization of the steady states in which the polymer grades are to be produced and the transition policies between them (Yi et al., 2003), but they treated these two tasks sequentially, that is, the influence of the optimal steady states on the grade transition was not analyzed. The more interesting problem of studying how the selected steady-states influence the operability of the grade changeover has rarely been explored. In this situation one might find a sub-optimal, though still reasonable steady state, that allowed a much easier grade transition, resulting in a better process performance as a whole.

Transition policies can only be carried out under well-controlled operating conditions. Different control designs have been proposed for polymerization processes, from classical PID controllers to modern nonlinear model predictive control (NLMPC) schemes (Embiruçu et al., 1996). Actually, a well designed control system is essential to implement the optimally determined dynamic trajectories in the presence of process disturbances and model uncertainties. This is particularly important because plant safety is a major issue during grade transition. Overshoots/undershoots are commonly performed to reduce transition time, and this can lead to process runaway. Therefore, several authors combined grade transition optimization with process control (Chatzidoukas et al., 2003; Wang et al., 2000; Na and Rhee, 2002; Bindlish and Rawlings, 2003; BenAmor et al., 2004). In most of these works, a sequential approach has been used to deal with control system design and grade transition optimization. For instance, Wang et al. (2000) applied a sequential strategy to an ethylene slurry polymerization reactor, where first an off-line optimizer calculated optimal transition policies. Then, a NLMPC scheme was used to implement the optimal transition policies in face of uncertainties in model parameters. Na and Rhee (2002) used a multivariable NLMPC for set point tracking in a styrene solution polymerization. Instead of first principle models, a polynomial auto-regressive moving average model (ARMA) was used to describe the nonlinear behavior of the polymerization reactor. This approach provided satisfactory control after set point changes in conversion and/or weight average molecular weight. These authors did not optimize transition policies. Bindlish and Rawlings (2003) developed a target linearization model predictive controller (TLMPC) to deal with plant start up, grade transition and regulatory control of a methyl methacrylate (MMA) and vinyl acetate (VA) copolymerization reactor with satisfactory results. These authors focused exclusively on process control. BenAmor et al. (2004) described the application of an industrial real time optimization package (ROMeo) to the NLMPC of a polymer grade transition. They applied their algorithm to methyl methacrylate and ethylene polymerization processes. The control scheme showed good performance for grade changes and disturbance rejection in the presence of model errors. As this study focused exclusively on the control problem, it was assumed that suitable trajectories of process outputs and inputs (i.e., optimal transition policies) were available.

The sequential approach to process design and control does not take into account that process control is an inherent property of process design, and that there is a strong interaction between them. Several works in other fields of chemical engineering have demonstrated the necessity of integrating process design and control (Bahri et al., 1997; Bansal et al., 2002). One of the few works to pursue this line in Polymer Science is that of Chatzidoukas et al. (2003), who performed a simultaneous process optimization and control, specifically control structure selection and grade transition optimization in a gas-phase olefin copolymerization reactor. However, they did not include equipment design and steady-state operating conditions in their optimization problem.

In this work a mixed-integer dynamic optimization (MIDO) approach is applied to the simultaneous design and control of a continuous styrene polymerization process. Here "process design" refers to the selection of the continuous stirred tank reactor (CSTR) unit, the peroxide initiator, and the steady-state operating points. With polymer grades as the only specifications, the process is designed to achieve optimal steady-state operation and grade transition policies. Unlike many previous grade transition studies, steady states are not known beforehand. In this case, they are determined so as to minimize capital and steady-state operating costs, as well as off-specification product during grade transition. At the same time, transition policies are designed so as to minimize transition time and off-specification polymer properties. As these two objectives might

be in conflict, trade-off between them is analyzed solving a multiobjective optimization. Simultaneously with the process design, a multivariable feedforward–feedback control scheme is optimally designed to drive the process from one operating point to the other. This task includes optimal pairings between controlled and manipulated variables and controller's tuning parameters for the PI feedback controllers, and the best control trajectories of the feedforward controllers.

To the best of our knowledge, the integration of process design, including equipment design, initiator selection, steady-state operating points and transition policies, with the control system design has not been addressed before for polymerization systems.

2. Process description and modeling aspects

Solution polymerization of styrene in continuous processes is often carried out using a combination of different reactor types. In a typical plant, the mixture of styrene, solvent and initiator goes through several polymerization units connected in series, each of them equipped with an agitator and appropriate heat-exchange systems. The output is then pumped to a devolatilizer unit to separate the unreacted monomer and the solvent. The hot viscous polymer is then pelletized and finally packaged (Simon and Chappelear, 1979). Usually, CSTRs are appropriate in the first stages, operating at low conversions to ensure moderate viscosities. Then, the polymerization is continued in other reactors, such as linear flow reactors, so as to reach higher conversions (Simon and Chappelear, 1979). As a first step, due to the complexity of the mathematical problem involved in this study, only a first stage CSTR will be considered in the present process design and control analysis. In this way the advantages of the employed methodology are clearly illustrated. Since all the pieces of equipment involved in the process work together and are interdependent, forthcoming work will address the extremely challenging problem of applying this approach to an entire plant.

Fig. 1 shows a schematic representation of the reactor for modeling purposes. Please notice that this is only a diagram and does not intend to reproduce a real reactor configuration. Monomer, initiator and solvent streams compose the reactor feed stream. Reactor output consists of polystyrene, unconverted monomer, initiator and solvent. Cooling water is used to remove the heat released by the polymerization.

In this work, a previous mathematical model (Hidalgo and Brosilow, 1990; Russo and Bequette, 1998) for styrene solution polymerization is extended to take into account the specific characteristics of the process under study and to add new predictive capabilities. The following reactions are considered: initiator decomposition, chain initiation, propagation and termination by combination. In the original model monomer thermal initiation and gel effect were neglected. The operating condition for the solvent fraction of 50% reported by Hidalgo and Brosilow (1990) will be used in this work, as this allows neglecting the gel effect (Choi, 1986). On the contrary, monomer thermal initiation (Asteasuain et al., 2003) has been included in the present model since it may become important at temperatures close to 100 °C. The calculation of the second moment of the polymer MWD has also been added in order to be able to predict the polymer weight average molecular weight and polydispersity. It should be mentioned that similar models of this system in which three moments of the polymer MWD are calculated, have also been reported in the literature (Prasad et al., 2002; Fontoura et al., 2003). Although model parameters may vary with time in polymerization processes (for instance the heat-transfer coefficient), for the present design and control problem, an inherent off-line analysis, average values are used. Therefore, density, specific heat and other physical properties of the reacting mixture are considered constant. Quasi-steady state of living radicals is also assumed. Details about the remaining model assumptions and the methodology of mass balances formulation can be found in Hidalgo and Brosilow (1990) and in Russo and Bequette (1998). For these model assumptions, the resulting mass balance equations that describe the process are shown in Table 1 (Eqs. (1)–(8)). Polymerization rate, conversion, polymer number (Mn) and weight (Mw) average molecular weights, and polydispersity, are calculated according to (Eqs. (9)–(13)) in Table 1. To model the heat transfer between the reacting mixture and the cooling fluid, it is assumed that the heat-transfer coefficient is constant. For the different reactor units, the product (UA) can be calculated as shown in Table 1 (Eq.(14)). $(UA)_0$ is the value of the product (UA) employed in the work by Hidalgo and Brosilow (1990), corresponding to a reactor of volume $V_0 = 3000\,\mathrm{L}$. In order to improve the efficiency of the numerical methods, the model equations are converted to a dimensionless form obtained by means of the dimensionless variables defined in Table 2. The

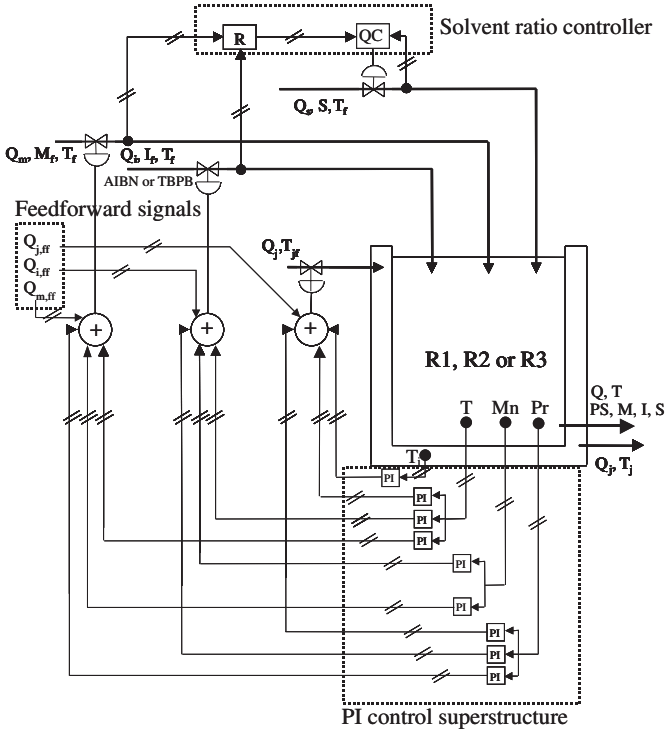

Fig. 1. Polymerization reactor scheme including control superstructure.

Table 1
Process model equations

$$\frac{dI}{dt} = \frac{1}{V}(Q_i I_f - QI) - k_{dI} I \quad (1)$$

$$\frac{dM}{dt} = \frac{1}{V}(Q_m M_f - QM) - k_p M \lambda_0 - 3k_{dM} M^3 \quad (2)$$

$$\frac{dT}{dt} = \frac{Q}{V}(T_f - T) + \frac{(-\Delta H_r)}{\rho Cp} - k_p M \lambda_0 - \frac{UA}{\rho Cp V}(T - T_j) \quad (3)$$

$$\frac{dT_j}{dt} = \frac{Q_j}{V_j}(T_{j,f} - T_j) + \frac{UA}{\rho_j Cp_j V_j}(T - T_j) \quad (4)$$

$$\frac{dM_0}{dt} = \frac{1}{2}k_{tc}\lambda_0^2 - \frac{Q}{V}M_0 \quad (5)$$

$$\frac{dM_1}{dt} = k_{tc}\lambda_0^2 + k_p M \lambda_0 - \frac{Q}{V}M_1 \quad (6)$$

$$\frac{dM_2}{dt} = 2k_{tc}\lambda_0^2 + 5k_p M \lambda_0 + 3\frac{k_p^2}{k_{tc}}M^2 - \frac{Q}{V}M_2 \quad (7)$$

$$\lambda_0 = \sqrt{\frac{2\text{effic}\, k_{dI} I + 2k_{dM} M^3}{k_{tc}}} \quad (8)$$

$$Pr = k_p M \lambda_0 \quad (9)$$

$$x = \frac{M_1}{M_1 + M} \quad (10)$$

$$Mn = Mw_M \frac{M_1}{M_0} \quad (11)$$

$$Mw = Mw_M \frac{M_2}{M_1} \quad (12)$$

$$Pd = \frac{Mw}{Mn} \quad (13)$$

$$(UA) = (UA_0)\frac{A}{A_0} \quad (14)$$

numerical values of the different model parameters are listed in Table 3.

2.1. Product specifications and process constraints

Product requirements include grade specifications defined as number average molecular weight (*Mn*), which must be satisfied at both steady states. For this work polymer grade A is defined as Mn_A=50 000 g mol^{-1}, and grade B as Mn_B=40 000 g mol^{-1}.

Table 2
Dimensionless variables

$\overline{I}=\frac{I}{I_{f0}}$	$\overline{M}=\frac{M}{M_{f0}}$	$\overline{I}_f=\frac{I_f}{I_{f0}}$	$\overline{M}_f\,\frac{M_f}{M_{f0}}$	$\overline{T}=\frac{T-T_{f0}}{T_{f0}}$
$\overline{T}_j=\frac{T_j-T_{f0}}{T_{f0}}$	$\overline{T}_f=\frac{T_f-T_{f0}}{T_{f0}}$	$\overline{T}_{j,f}=\frac{T_{j,f}-T_{f0}}{T_{f0}}$	$\overline{M}_0=\frac{M_0}{M_{f0}}$	$\overline{M}_1=\frac{M_1}{M_{f0}}$
$\overline{Q}_i=\frac{Q_i}{Q_0}$	$\overline{Q}_m=\frac{Q_m}{Q_0}$	$\overline{Q}_s=\frac{Q_s}{Q_0}$	$\overline{Q}=\frac{Q}{Q_0}$	$\overline{t}=\frac{Q_0 t}{V_0}$

Table 3
Model parameters

effic	0.6[a]	$\rho_j Cp_j$	4045.7048 J L^{-1} K^{-1}[a]
$A_{d,\text{AIBN}}$	5.95×10^{13} s^{-1}[a]	$I_f=I_{fo}$	0.5888 mol L^{-1}[a]
$E_{d,\text{AIBN}}$	123853.658 J mol^{-1}[a]	$M_f=M_{f0}$	8.6981 mol L^{-1}[a]
$A_{d,\text{TBPB}}$	8.439×10^{13} s^{-1}[b]	T_{f0}	330 K
$E_{d,\text{TBPB}}$	133888 J mol^{-1}[b]	Q_0	0.2625 L s^{-1}
A_p	1.06×10^7 L mol^{-1} s^{-1}[a]	Mw_M	104.15 g mol^{-1}
E_p	29572.898 J mol^{-1}[a]	Mw_{AIBN}	164.2 g mol^{-1}
A_{tc}	1.25×10^9 L mol^{-1} s^{-1}[a]	Mw_{TBPB}	194.2 g mol^{-1}
E_{tc}	7008.702 J mol^{-1}[a]	a	3.1536×10^7 s year^{-1}
V_0	3000 L	c_1	1.32 10^{-4} \$ L^{-1}[c]
$-\Delta H_r$	69919.56 J mol^{-1}[a]	c_2	1.1 10^{-2} \$ g^{-1}[d]
UA_0	293.076 J s^{-1} K^{-1}[a]	c_3	7.5 10^{-3} \$ g^{-1}[d]
ρCp	1507.248 J L^{-1} K^{-1}[a]		

[a] Russo and Bequette (1998).
[b] Kim (1991).
[c] Schweiger and Floudas (1997).
[d] Personal communication with Akzo Nobel Polymer Chemicals, Argentina, 2004.

As in this work we limit the design to the prepolymerization CSTR unit, we define as acceptable conversion limits for this intermediate stage the values indicated in Eq. (15). The lower bound in steady-state conversion is selected to ensure profitable production, and the upper bound to avoid high-viscosity mixtures

$$0.18 \leqslant x_A, x_B \leqslant 0.50. \quad (15)$$

In order to maintain the operating range within the bounds where the model parameters were obtained, upper bounds for the reactor temperature were set. Those bounds were selected as 100 and 110 °C for the steady-state and the grade transition operations, respectively. Another important point to consider is that this type of process usually presents steady-state multiplicity. In order to exclude low conversion steady states, a lower bound of 70 °C for the steady-state reactor temperature was selected. These temperature bounds are within the range of those employed for the first stage polymerizer in several industrial styrene polymerization processes (Simon and Chappelear, 1979; US Patents, 1981, 1992, 1994). Steady-state temperatures for production of both polymer grades (A and B) and reactor temperature during transition must then verify Eqs. (16) and (17), respectively,

$$70\,^\circ\text{C} \leqslant T_A, T_B \leqslant 100\,^\circ\text{C}, \quad (16)$$

$$T(t) \leqslant 110\,^\circ\text{C}. \quad (17)$$

Besides, an upper limit for the jacket temperature at any time was selected so as to keep a safety margin with respect to the boiling point of water, as shown in Eq. (18)

$$T_j(t) \leqslant 95\,^{\circ}\mathrm{C}. \tag{18}$$

Notice that reactor and jacket temperature constraints (Eqs. (17) and (18)) during grade transition are path constraints. This class of constraint was dealt with by converting them into end-point constraints, following the procedure reported by Bansal et al. (2002).

Bounds for the coolant flow rates at steady states were set as shown in Eq. (19). These limits result from setting a range around the value of a base case reported by Russo and Bequette (1998):

$$0.079\,\mathrm{L\,s^{-1}} \leqslant Q_{j,\mathrm{A}},\ Q_{j,\mathrm{B}} \leqslant 0.26\,\mathrm{L\,s^{-1}}. \tag{19}$$

Additional process restrictions involve monomer flow rate at steady states and cooling fluid inlet temperature, which are fixed at $0.105\,\mathrm{L\,s^{-1}}$ and $22\,^{\circ}\mathrm{C}$, respectively. The feed temperature is not known in advance, but it should be the same at both steady states. An upper bound for this variable was set in order to keep it within the typical values reported in the literature, as shown in Eq. (20)

$$T_f \leqslant 67\,^{\circ}\mathrm{C}. \tag{20}$$

3. Simultaneous process design and control problem

Even though it is not unusual for a polymer plant to produce more than 30 polymer grades, the analysis in this work is limited to a transition between two polystyrene grades as a way to test the methodology. Specifically, transition from grade A to grade B production is considered. Transition from grade B to A is also analyzed. Three different situations are considered. First, the plant is producing grade A polymer since the start-up and will make only one grade transition to grade B, which will be produced up to a plant shut-down. In second place, the inverse situation is analyzed (producing grade B polymer from start-up, changing to grade A polymer at a certain moment). Finally, periodical grade changes between grades A and B without intermediate shut-downs are studied. In order to make the three cases comparable, exactly 50% of the time is devoted to the production of each polymer grade in all three scenarios. Process design should yield economically optimal steady states in terms of capital and operating costs. At the same time, the grade transition will be optimized to minimize off-specification product. Therefore, the design problem constitutes a multiobjective optimization. The ε-constraint method (Tsoukas et al., 1982) is used to deal with this multiobjective optimization. This method presents the important advantage of allowing comparisons of trade-offs between design objectives.

Process design includes the selection of optimal reactor size, initiator, and steady-state operating points at which the polymer grades are produced. The process and the control system for the grade transition are designed simultaneously. A multivariable control scheme is considered that allows a combination of feedforward and feedback controllers. The control scheme is outlined in Fig. 1. The design solution provides the optimal trajectories for the feedforward controllers. For the feedback controllers, the "best" pairings between controlled and manipulated variables, from the control superstructure, as well as controllers' tuning parameters, are determined.

3.1. Process design variables

Process design includes the reactor unit, selection of initiator, and the steady-state operating points. Two of these process design items involve discrete decisions. One of them is the polymerization reactor. We assume that from previous process analysis and equipment availability, the selection has to be made from the following three alternatives:

$R1: V = 2000\,\mathrm{L}$,	$R2: V = 3000\,\mathrm{L}$,	$R3: V = 3500\,\mathrm{L}$,
$V_j = 2208\,\mathrm{L}$,	$V_j = 3312\,\mathrm{L}$,	$V_j = 3864\,\mathrm{L}$,
$A/A_0 = 0.763$,	$A/A_0 = 1$,	$A/A_0 = 1.108$.

These are typical dimensions of this type of units as reported in the literature (Hidalgo and Brosilow, 1990). Therefore, the reactor volume is modeled as a discrete variable with only three possible values. The jacket volume verifies a constant relationship to the reactor volume, that is

$$\frac{V_j}{V} = 1.104. \tag{21}$$

This ratio corresponds to the data reported in Hidalgo and Brosilow (1990).

The other discrete decision is the initiator type. Through an appropriate initiator selection, it is possible to enhance reactor performance to increase production, achieve certain molecular properties or improve controllability. Our model may consider any finite number of initiators that can be selected either alone or mixed. In this work, the initiators allowed are azobis(isobutyronitrile) (AIBN) and *tert*-butyl peroxybenzoate (TBPB). AIBN is more reactive than TBPB but its cost is higher. Initiator selection is modeled by means of binary variables (y_{AIBN} and y_{TBPB}). These variables are employed to select the pre-exponential factor and the activation energy of the initiator decomposition constant corresponding to the chosen initiator:

$$A_d = A_{\mathrm{AIBN}} y_{\mathrm{AIBN}} + A_{\mathrm{TBPB}} y_{\mathrm{TBPB}}, \tag{22}$$

$$E_d = E_{\mathrm{AIBN}} y_{\mathrm{AIBN}} + E_{\mathrm{TBPB}} y_{\mathrm{TBPB}}, \tag{23}$$

$$y_{\mathrm{TBPB}} + y_{\mathrm{AIBN}} = 1. \tag{24}$$

The integer constraint represented by Eq. (24) was included to specify that, for this particular design, it is desired to use only one initiator. Besides, for the third situation analyzed, the cyclic transitions between grades A and B, the same peroxide must be used for both transitions.

The description of the process without considering the control system comprises 37 equations: a set of 30 equations, 15 for each of the two steady states, that includes Eqs. (1)–(13) and the specified values for Mn and Q_m, together with Eqs. (14), (21)–(24), the relation between the transfer area and

its nominal value, and the imposition that the feed temperatures must be equal at both steady states. These 37 equations involve 42 variables (the set of Q_i, Q_m, Q_j, x, I, M, M_0, M_1, M_2, λ_0, T, T_j, T_f, Mw, Mn, Pr, and Pd at each of the two steady states, together with V, V_j, UA, A/A_0, A_d, E_d, y_{AIBN}, and y_{TBPB}). This results in five degrees of freedom, so there can be up to five process optimization variables. Two of them were already selected, as mentioned above (V, and y_{AIBN} or y_{TBPB}). The remaining three process decision variables selected were the reactor temperatures at each of the two steady states (T_{A}, T_{B}) and the coolant flow rate at steady state A ($Q_{j\mathrm{A}}$). This simplifies the inclusion of some process constraints in the optimization problem, and also the solution of the nonlinear equations corresponding to the steady-state operating points.

3.2. Control system design variables

In order to find the best control system that would drive the process from one steady state to the other, a multivariable control scheme is analyzed. Reactor and jacket temperatures, polymerization rate and *Mn* are considered as possible controlled variables. *Mn* was selected as controlled variable, although *Mw* might have been chosen as well. As the polydispersity index presents small variations in styrene solution polymerization, control objectives can be formulated in terms of either *Mn* or *Mw* (Fontoura et al., 2003). Online size exclusion chromatography (SEC) devices are available that provide online measurements of the average molecular weights. However, these measurements involve a delay that ranges between 10 and 40 min (Ellis et al., 1994). To overcome this problem, Kalman filters have been employed to provide online estimates of the molecular weights between SEC measurements. Successful molecular weight control schemes have been implemented in this way (Kim, 1991; Ellis et al., 1994; Prasad et al., 2002). Kalman filters or empirical correlations have also been used in combination with online sensors of reaction mixture properties other than molecular weights, to obtain online estimates of the molecular weights for control purposes (Fontoura et al., 2003; Ponnuswamy et al., 1987). Therefore, in this article it is assumed that online values of the polymer *Mn*, as well as reactor and jacket temperatures and polymerization rate, are readily available for the controllers by means of an appropriate online device.

The variables that could be manipulated in this reactor are: monomer, initiator and coolant flow rates. In solution polymerization, solvent volume fraction should be kept approximately constant (Hidalgo and Brosilow, 1990). Therefore, a ratio controller is used to maintain a constant solvent volume fraction of 50%. This value, which is approximately the one reported by Hidalgo and Brosilow (1990), is high enough to allow neglecting the gel effect. Then, the solvent flow rate is related to the monomer and initiator flow rates as

$$Q_s = Q_i + Q_m. \tag{25}$$

The solvent ratio controller and a combination of feedforward and feedback controllers compose the proposed control system: feedforward controllers for property control (*Mn*) and feedback PI controllers for reactor and jacket temperatures, polymerization rate and *Mn* control. For this work it was established that feedforward controllers must manipulate all control efforts, but optimal matching between manipulated and controlled variables for the PI controllers should be determined.

The overall control action on each manipulated variable is composed by the action of the feedforward controller and of each feedback loop in which the variable is involved. Hence, the control superstructure can be represented by Eq. (26)

$$U_i^* = U_{i,\mathrm{ff}} + \sum_{j=1}^{4} K_{i,j}\left[(Y_{j,\mathrm{set}} - Y_j) + \frac{1}{\tau_{i,j}}\int_0^t (Y_{j,\mathrm{set}} - Y_j)\,\mathrm{d}t'\right]. \tag{26}$$

U_i^* is the overall control action on the ith manipulated variable ($U_1^* = Q_j^*, U_2^* = Q_i^*, U_3^* = Q_m^*$), and Y_j is the jth controlled variable ($Y_1 = T, Y_2 = T_j, Y_3 = Mn, Y_4 = Pr$); $Y_{j,\mathrm{set}}$ is the set point of the Y_j variable. $U_{i,\mathrm{ff}}$ stands for the feedforward controller's action. The terms in the sum represent the action of the PI controllers over the ith manipulated variable.

It should be noted that Eq. (26) represents the control superstructure, and therefore it includes all *potential* PI loops between controlled and manipulated variables. Which of these loops will actually compose the final control system is part of the design problem. If any of the manipulated variables is not matched with a given controlled variable, the corresponding term of the PI controller in Eq. (26) should vanish. This is modeled using binary variables as follows:

$$K_{i,j}^{lb} y_{i,j} \leqslant K_{i,j} \leqslant K_{i,j}^{ub} y_{i,j}. \tag{27}$$

The binary variable $y_{i,j}$ takes the value of 1 if the ith manipulated variable is matched with the jth controlled variable, or 0 otherwise. The control superstructure yields $2^{12} = 4096$ control alternatives, identified by the 12 binary variables. However, some of these options were disregarded in advance based on process knowledge and previous simulations. For example, it is not reasonable to control jacket temperature manipulating monomer or initiator flow rates. Besides, previous simulation results showed that the combination Q_j–*Mn* did not result in an effective control action. This type of considerations results in the following decisions previous to the actual optimization:

- Not controlling T_j by manipulating Q_i ($y_{2,2} = 0$).
- Not controlling T_j by manipulating Q_m ($y_{3,2} = 0$).
- Not controlling *Mn* by manipulating Q_j ($y_{1,3} = 0$).

In this way, the combinatorial size of the optimization problem was reduced in 3584 discrete alternatives ($2^{12} - 2^9 = 3584$). No restrictions are imposed on the number of loops in which any manipulated or controlled variable can be involved. It should be noted that multivariable PI schemes in which a single manipulated variable is employed in more than one control loop have been reported in the literature (Wang, 2003; Kookos and Perkins, 2001; Chatzidoukas et al., 2003).

Table 4
Constraints on the manipulated variables during grade transitions

Manipulated variable	Lower bound ($L\,s^{-1}$)	Upper bound ($L\,s^{-1}$)
Q_j	0	41
Q_i	0	0.066
Q_m	0	1.31

In order to take into account constraints on the manipulated variables, the following saturation function was defined

$$U_i = \begin{cases} U_{i,\max} & \text{if } U_{i,\max} < U_i^*, \\ U_i^* & \text{if } U_{i,\min} \leqslant U_i^* \leqslant U_{i,\max}, \\ U_{i,\min} & \text{if } U_i^* < U_{i,\min}. \end{cases} \quad (28)$$

We developed the following expression so as to smooth Eq. (28)

$$\begin{aligned} U_i = {} & 0.25[(U_i^* - U_{i,\min})\tanh(\xi(U_i^* - U_{i,\min})) + U_i^* + U_{i,\min}] \\ & \times [\tanh(\xi(U_{i,\max} - U_i^*)) + 1] \\ & + 0.5U_{i,\max}[\tanh(\xi(U_{i,\max} - U_i^*)) + 1]. \end{aligned} \quad (29)$$

Parameter ξ determines the "smoothness" of the expression defined by Eq. (29). The larger the ξ is, the more Eq. (29) resembles Eq. (28). Here we used $\xi = 10^6$. $U_{i,\min}$ and $U_{i,\max}$ values are reported in Table 4.

Feedforward controller's actions ($U_{i,\mathrm{ff}}$), controlled variables' set points ($Y_{j,\mathrm{set}}$), binary variables representing the matching between controlled and manipulated variables ($y_{i,j}$) and the PI controllers' tuning parameters ($K_{i,j}$ and $1/\tau_{i,j}$), are determined in the same optimization run, simultaneously with the process design variables. The objective functions aim at minimizing off-specification material and transition time, and steady-state operating costs. At the same time, process safety constraints must be satisfied. In this way, an optimal design for the process and the control system as a whole is obtained. As all the elements of the control system are designed simultaneously, all possible interactions between the different loops are taken into account. It should be noted that no simplification of the process model is carried out in order to design the control system. The optimizer calculates each of the time profiles for $Y_{j,\mathrm{set}}$ and $U_{i,\mathrm{ff}}$ as a series of piecewise constant values. The PI controllers' tuning parameters ($K_{i,j}$ and $1/\tau_{i,j}$) are considered time invariant optimization variables.

3.3. Objective functions

One of the design objectives for steady-state operation is minimizing costs for production of grade A and B polymers. The cost function comprises an annualized reactor cost, and an average of the operating costs for producing polystyrenes of grade A and B:

$$C[\$\,\mathrm{year}^{-1}] = \tfrac{1}{4}C_R + \tfrac{1}{2}(C_{\mathrm{op,A}} + C_{\mathrm{op,B}}). \quad (30)$$

C_R is the reactor cost, which is annualized considering a four-year amortization (Schweiger and Floudas, 1997). It is calculated as

$$C_R[\$] = 343.16V^{0.529}. \quad (31)$$

Eq. (31) was determined fitting cost data for a stirred jacket reactor (material: carbon steel, operating pressure: atmospheric to 25 psi) (Matches, 2004). Thirteen points corresponding to reactor volumes ranging from 2000 to 3500 L were used to obtain the cost equation, which provides a very good fit ($R^2 = 0.9999$).

$C_{\mathrm{op,A}}$ and $C_{\mathrm{op,B}}$ are the operating costs when producing grade A and B, respectively. $C_{\mathrm{op,A}}$ and $C_{\mathrm{op,B}}$ comprise coolant (C_{cool}) and initiator (C_{in}) costs, which are shown in Eqs. (32) and (33), respectively. Binary variables are used to include only the cost of the selected initiator in the objective function. Values for parameters a, c_1, c_2 and c_3 are shown in Table 3

$$C_{\mathrm{cool}}[\$\,\mathrm{year}^{-1}] = c_1 a(Q_{j,\mathrm{A}} + Q_{j,\mathrm{B}})[L\,s^{-1}], \quad (32)$$

$$\begin{aligned} C_{\mathrm{in}}[\$\,\mathrm{year}^{-1}] = {} & (c_2 Mw_{\mathrm{AIBN}} y_{\mathrm{AIBN}} + c_3 Mw_{\mathrm{TBPB}} y_{\mathrm{TBPB}}) \\ & \times I_f a(Q_{i,\mathrm{A}} + Q_{i,\mathrm{B}})[L\,s^{-1}]. \end{aligned} \quad (33)$$

The objective function for grade transition optimization measures the integral over time of the squared difference between the Mn of the target grade and the Mn of the polymer being produced at time t. That is,

$$Gt = \int_0^{t_f} (Mn_{\mathrm{Target}} - Mn(t))^2\,\mathrm{d}t. \quad (34)$$

For A to B transition, $Mn_{\mathrm{Target}} = Mn_{\mathrm{B}}$ and $Mn(0) = Mn_{\mathrm{A}}$; for B to A transition, $Mn_{\mathrm{Target}} = Mn_{\mathrm{A}}$ and $Mn(0) = Mn_{\mathrm{B}}$. An objective function like Eq. (34) not only minimizes an off-specification property, but also the transition time because the upper limit of the integral in Eq. (34) (t_f) is treated as an additional optimization variable (Chatzidoukas et al., 2003).

In the third situation considered, the cyclic transitions from A to B and B to A, designs for each transition cannot be treated as two different optimization problems, because they share some of the optimization variables, i.e., reactor unit and peroxide initiator selections, and the steady-state operating points. A single optimization problem that takes into account both transitions simultaneously must be solved instead. In order to tackle this problem, "twin" sets of process model equations were defined. One of them represents the process going from grade A to grade B operating point, and the other the opposite transition. Both sets of differential and algebraic equations are solved together from the initial time up the final time horizon (t_f). The initial condition for the first set is the steady-state point of grade A production, while grade B operating point is the target steady-state; the opposite holds for the second set. The only connections between the "twin" sets are the optimization variables mentioned before. Eq. (34) was modified so as to include both transitions in the objective function. Then, the new objective

function for the third situation is

$$Gt = \int_0^{t_{f,\mathrm{AB}}} (Mn_{\mathrm{B}} - Mn_{\mathrm{AB}}(t))^2 \,\mathrm{d}t + \int_0^{t_{f,\mathrm{BA}}} (Mn_{\mathrm{A}} - Mn_{\mathrm{BA}}(t))^2 \,\mathrm{d}t. \quad (35)$$

Mn_{A} and Mn_{B} are the number average molecular weights of grades A and B, respectively, and $Mn_{\mathrm{AB}}(t)$ and $Mn_{\mathrm{BA}}(t)$ are, respectively, the number average molecular weights in the first and second sets.

Operating costs are not included in the grade transition objective function because minimizing off-specification polymer is by far more important than reducing operating costs during this operation (Yi et al., 2003).

4. Optimization problem formulation

The simultaneous process-control system designs that have been presented constitute multiobjective mixed-integer dynamic optimization (MIDO) problems, which can be posed as follows:

$$\min_{u(t),z,d,y,t_f} \begin{bmatrix} C(x_a^*, z, y, d, p) \\ Gt(x_d(t_f), x_a(t_f), x_a^*, z, u(t_f), y, d, p) \end{bmatrix}$$

s.t.

$$h_d(\dot{x}_d(t), x_d(t), x_a(t), x_a^*, z, u(t), y, d, p) = 0,$$

$$h_d(x_d(t), x_a(t), x_a^*, z, u(t), y, d, p) = 0,$$

$$h_0(\dot{x}_d(0), x_d(0), x_a(0), x_a^*, z, u(0), y, d, p) = 0,$$

$$h_y(y) = 0,$$

$$g_e(\dot{x}_d(t_f), x_d(t_f), x_a(t_f), x_a^*, z, u(t_f), y, d, p) \leqslant 0,$$

$$g_q(x_a^*, z, y, p) \leqslant 0,$$

$$u^{lb} \leqslant u(t) \leqslant u^{ub},$$

$$z^{lb} \leqslant z \leqslant z^{ub},$$

$$y \in \{0, 1\}^{11 \text{ or } 20},$$

$$d \in D,$$

$$0 \leqslant t \leqslant t_f. \quad (36)$$

h_d and h_a are the closed-loop model differential-algebraic system; h_0 is the set of initial conditions; h_y are the pure integer equalities; g_e and g_q are the end-point and time-invariant inequalities, respectively, and D is a set of three discrete values representing allowed reactor sizes. The set h_a includes the model differential equations set to zero, in order to define both steady states. x_d are the differential state variables, $x_a(t)$ and x_a^* are the time variant and time invariant algebraic variables, respectively; p are the model parameters; $u(t)$ is the set of time-varying optimization variables (seven elements in the first and second cases ($Y_{j,\mathrm{set}}$, $j = 1$–4, $U_{i,\mathrm{ff}}$, $i = 1$–3) and 14 in the third case ($Y_{j,\mathrm{set}}$ and $U_{i,\mathrm{ff}}$ for the "twin" sets)), z is the set of time-invariant decision variables (29 elements in the first and second cases ($K_{i,j}$ and $1/\tau_{i,j}$ (18 variables), T_{A}, T_{B}, $Q_{j,\mathrm{A}}$ and the length of the eight time intervals used to divide the time horizon), and 47 in the third case (T_{A}, T_{B}, $Q_{j,\mathrm{A}}$ and the length of the eight time intervals (11 variables), and $K_{i,j}$ and $1/\tau_{i,j}$ for the "twin" sets (36 variables)); y is a set of binary variables (11 in the first and second cases ($y_{i,j}$ (nine variables), y_{AIBN} and y_{TBPB}) and 20 in the third case ($y_{i,j}$ for the "twin" sets, y_{AIBN} and y_{TBPB})); d is a discrete variable (reactor volume). Additional constraints were also included involving controlled and manipulated variables, and time derivatives for the state variables. These constraints ensured that the target steady-state operating point was actually reached. The resulting MIDO was solved following the strategy outlined below.

The multiobjective optimization is solved in this work by employing the ε-constraint method. It implies formulating Eq. (36) as a single objective optimization problem, incorporating the second function as an inequality constraint. In this case,

$$\min_{u(t),z,d,y,t_f} \quad Gt$$

s.t.

$$C \leqslant \varepsilon,$$

$$\varepsilon \in [\varepsilon_{\min}, \varepsilon_{\max}]. \quad (37)$$

Eq. (37) is solved for different values of ε in order to generate the non-inferior or Pareto set. This set is composed by all feasible points (that is, where all constraints are satisfied) among which no improvement on one objective function can be made without simultaneously worsening the other. From this set, the final solution can be chosen according to a subjective criterion.

In order to determine $\varepsilon_{\min}$ and $\varepsilon_{\max}$, Eq. (36) is solved separately for C and Gt, respectively. $\varepsilon_{\min}$ is the value of C obtained in the first optimization, and $\varepsilon_{\max}$ is the value of C in the second one. It should be noted that function C involves only variables associated with the steady states, reactor unit and type of initiator. Therefore, when solving Eq. (36) only for this function to calculate $\varepsilon_{\min}$, the optimization problem was decomposed in this way: first, all optimization variables and constraints related to the grade transition (including differential equations) were excluded, and the minimum value of C was obtained. Then, the value of Gt corresponding to this point was determined solving Eq. (36) for Gt only, but with the reactor unit, type of initiator and steady-state optimization variables fixed at the values obtained before.

The MIDO problems were solved with the gPROMS/gOPT package (Process Systems Enterprise Ltd.), which decomposes the MIDO into a Master problem (mixed-integer linear problem) in which the discrete optimization variables are updated, and a Dynamic optimization problem in which the remaining optimization variables are determined for a fixed set of the discrete variables (Process Systems Enterprise, Ltd., 2005). Dynamic optimization problems are solved in gPROMS by control vector parameterization. For this parameterization, the time horizon was divided into a fixed number of time intervals, as required by gPROMS. Eight time intervals were used in this work. It was verified that a larger number did not improve the

optimal solution. As mentioned before, the length of each of the time intervals was included in the set of optimization variables. Piecewise constant profiles were selected for the time varying optimization variables.

In the general case, the problem described by Eq. (36) can be highly nonlinear, and consequently susceptible of having local optimums. Taking into consideration that we are using a general deterministic optimization approach to solve it, we cannot guarantee finding the global solution among the possible local ones. However, to the authors' best knowledge, a well developed deterministic approach to find the global solution of a nonstructured problem of the type shown in Eq. (36) is yet to be found. On the other hand, evolutionary strategies, i.e., genetic algorithms, have been considered in the literature (Bhaskar et al., 2000; Guria et al., 2005) given their ability to approach the global optimum, even though they cannot guarantee finding the global solution in a general case either. Nevertheless, for the particular problem analyzed in this paper we tried multiple starting points when solving the optimization problems, and therefore we believe that the reported results are indeed global optimums.

5. Results and discussion

5.1. Transition from grade A to B polymer

After solving Eq. (36) for C only (to determine $\varepsilon_{\min}$), the design solution obtained for the transition from grade A to B polymer is shown in Table 5. Decision variables were reactor size and initiator type (discrete), T at both operating points and Q_j at grade A production (continuous); $T_{j,f}$ and Q_m were fixed in advance, and Q_s is related to Q_i and Q_m, as explained before. As may be seen, the smallest reactor is selected, which is consistent with capital cost reduction. However, the most expensive initiator turns out to be the best option. Evidently, the decomposition properties of this initiator allow smaller flow rates resulting in a lower cost. It is important to note that initiator cost represents approximately 95% of the overall cost. Conversion levels were similar for both A and B grades, falling in the middle of the range of accepted conversions.

When solving Eq. (36) for Gt only (to determine $\varepsilon_{\max}$), the grade transition optimization resulted in the same process design variables (steady-state operating points, reactor unit and initiator type) as in the previous optimization. This implies that the objectives are not in conflict since the minima for C and Gt coincide, resulting in only one point in the Pareto set. This type of coincidence, which may be surprising, has also been found by Bhat et al. (2004) when solving a multiobjective optimization for the continuous tower process for styrene polymerization. It is important to remark that the solution to this multiobjective optimization problem was thoroughly checked. First of all, the optimization was performed with multiple starting points, and the same solution was obtained each time. Secondly, the optimization was repeated but relaxing the specifications on Mn at both steady states ($Mn_{\mathrm{A}} = Mn_{\mathrm{A,desired}} \pm c$, $Mn_{\mathrm{B}} = Mn_{\mathrm{B,desired}} \pm c$). Although Pareto sets were obtained with the relaxed constraints, in all cases the points of the Pareto set lied at the bounds of the constraints $Mn_{\mathrm{A,B}} = Mn_{\mathrm{A,B,desired}} \pm c$. This means that none of these points was a solution to the problem of interest in this work ($Mn_{\mathrm{A,B}} = Mn_{\mathrm{A,B,desired}} \pm 0$). It was also found that when the value of c approached zero, the Pareto set points "moved" towards the unique solution we had previously found.

The value of the objective function for grade transition from A to B polymer is $Gt = 3.5 \times 10^{-4}$ at the optimum.

The optimal PI control structure is schematized in Fig. 2. The optimal controller parameters, gains and reset rates, are shown in Eqs. (38) and (39).

Table 5
Optimal steady-states design for AB grade transition

C : 105746 \$ year^{-1}		
Reactor volume: 2000 L Initiator: AIBN		
	Grade A	Grade B
T	100 °C	100 °C
T_f	66 °C	
T_j	54 °C	45 °C
Q_j	0.079 L s^{-1}	0.138 L s^{-1}
Q_i	2.51×10^{-3} L s^{-1}	3.48×10^{-3} L s^{-1}
Conversion	33%	37%

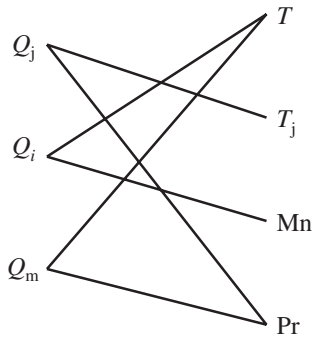

Fig. 2. Pairing between manipulated and controlled variables corresponding to the optimal design for the A to B transition.

$$K = \begin{bmatrix} \cdots & K_{1,2} = 7.95 \times 10^{-3}\,\mathrm{L\,s^{-1}\,K^{-1}} & \cdots & K_{1,4} = -416.15\,\mathrm{L\,s^{-1}\,g^{-1}\,s^{-1}} \\ K_{2,1} = 7.96 \times 10^{-6}\,\mathrm{L\,s^{-1}\,K^{-1}} & \cdots & K_{2,3} = -2.63 \times 10^{-5}\,\mathrm{L\,s^{-1}\,g^{-1}\,mol^{-1}} & \cdots \\ K_{3,1} = -7.96 \times 10^{-6}\,\mathrm{L\,s^{-1}\,K^{-1}} & \cdots & K_{3,3} = 2.38 \times 10^{-5}\,\mathrm{L\,s^{-1}\,g^{-1}\,mol^{-1}} & \cdots \end{bmatrix}, \quad (38)$$

$$\frac{1}{\tau} = \begin{bmatrix} \cdots & \frac{1}{\tau_{1,2}} = 8.75 \times 10^{-6}\,\mathrm{s^{-1}} & \cdots & \frac{1}{\tau_{1,4}} = 0 \\ \frac{1}{\tau_{2,1}} = 0 & \cdots & \frac{1}{\tau_{2,3}} = 8.75 \times 10^{-6}\,\mathrm{s^{-1}} & \cdots \\ \frac{1}{\tau_{3,1}} = 5.26 \times 10^{-7}\,\mathrm{s^{-1}} & \cdots & \frac{1}{\tau_{3,3}} = 1.01 \times 10^{-6}\,\mathrm{s^{-1}} & \cdots \end{bmatrix}. \quad (39)$$

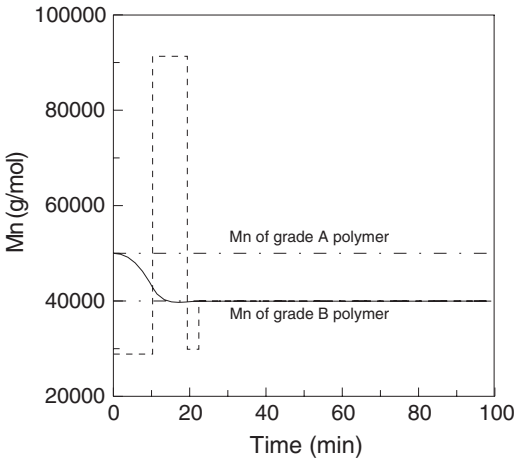

Fig. 3. *Mn* (—-) and *Mn* set point (- - -) profiles corresponding to the optimal design for the A to B grade transition.

Fig. 3 shows the *Mn* trajectory. It can be seen that the optimally designed control system drives *Mn* to the target value in a very short time, with negligible undershoot. As this property is kept almost constant thereon by the optimal control system, the amount of off-specification product is minimal. It must be kept in mind that the reactor residence time is approximately 2.5 h. The optimal profile of the *Mn* set point for the feedback controllers is presented in Fig. 3.

Figs. 4 (a) and (b) depict reactor and jacket temperature trajectories, respectively. It is interesting to see that the transient behavior of these variables shows large swings, particularly at the beginning of the grade transition. This is indeed the result of the appropriate control actions taken in order to achieve the control objectives of minimum off-specification material and transition time. The response of the control system can be interpreted in terms of the time profiles of the polymer *Mn* and the *Mn* set point. The initial 10-min period during which a sharp increase of 5 °C occurs, corresponds to the initial transition period in which the *Mn* set point is at its lowest value (see Fig. 3). The temperature increase aids in obtaining a fast transition because *Mn* lowers as temperature rises. During this period, about 70% of the total change in the polymer *Mn* is accomplished. Afterwards, a sudden decrease of 17 °C in the next 9 min occurs. This period corresponds to the one in which the *Mn* set point is at the highest value (see Fig. 3). This can be interpreted as the control system acting fast to minimize the undershoot in the polymer *Mn*, and therefore the reactor temperature is suddenly lowered. This period ends when the undershoot point of *Mn* during the grade transition occurs. The jacket temperature profile obviously resembles that of the reactor temperature. It should be noted that the maximum reactor and jacket temperature constraints of 110 and 95 °C, respectively, are satisfied along the reaction time. Notice the longer time needed to take the reactor and jacket temperatures to their steady-state values, in comparison with the time required for the polymer *Mn* to reach its steady-state value. It should be remembered, however, that the objective function for grade transition consisted only in minimizing off-specification *Mn*. This long time recovery of

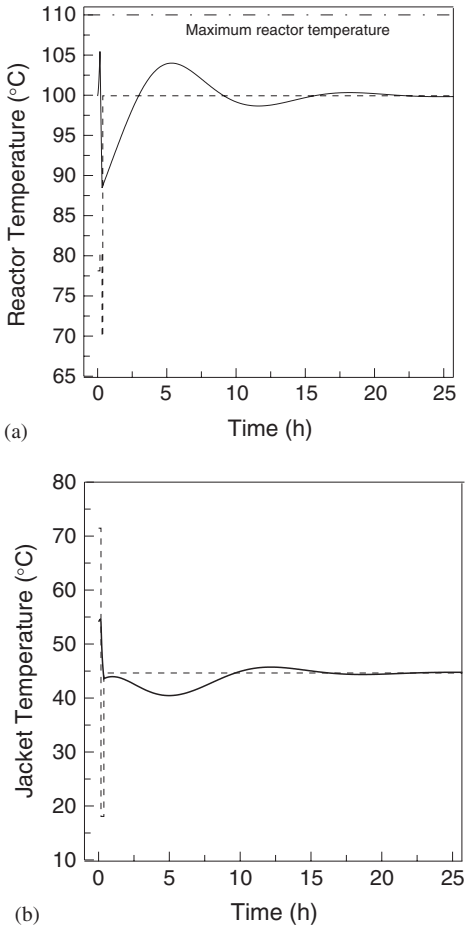

Fig. 4. Profiles of (a) the reactor temperature (—-) and the reactor temperature set point (- - -) - and (b) the jacket temperature (—-) and jacket temperature set point (- - -) corresponding to the optimal design for the A to B grade transition.

the reactor temperature and jacket temperatures is the best way to fulfill this objective.

Monomer and initiator concentration profiles during grade transition resemble those of the reactor temperature, although the slopes of the curves are always of the opposite sign since monomer and initiator consumptions increase with increasing temperatures. Although this polydispersity was not included in the design specifications, it presents a suitable behavior during the transition process. The start and end values of the polymer polydispersity correspond to the theoretical value of 1.5 for reactions involving propagation and termination by combination at constant temperature. When grade transition starts, the polydispersity increases slightly showing a maximum of less than 1.7, decreasing smoothly afterwards.

5.2. Transition from grade B to A polymer

In this case, the optimal designs for minimal *Gt* and *C* do not coincide. Fig. 5 shows the Pareto set for this transition. Each point corresponds to a different process and control system design, which varies from point 1, the design that yields the

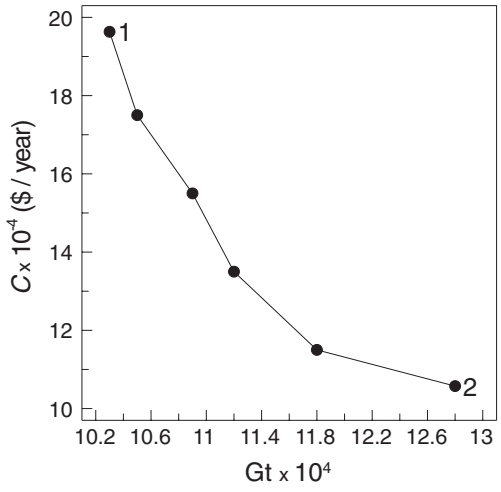

Fig. 5. Pareto set for the multiobjective optimization corresponding to the B to A grade transition design problem.

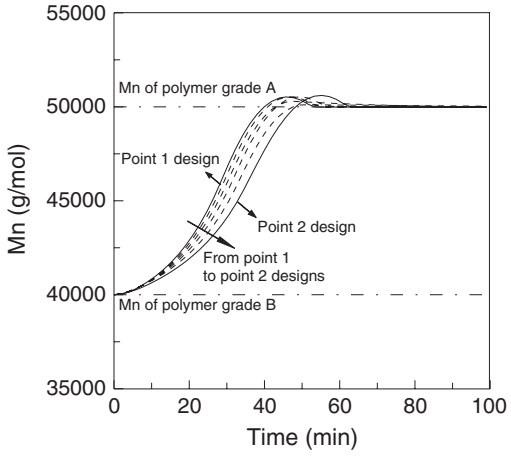

Fig. 6. *Mn* profiles corresponding to the optimal designs for the B to A grade transition.

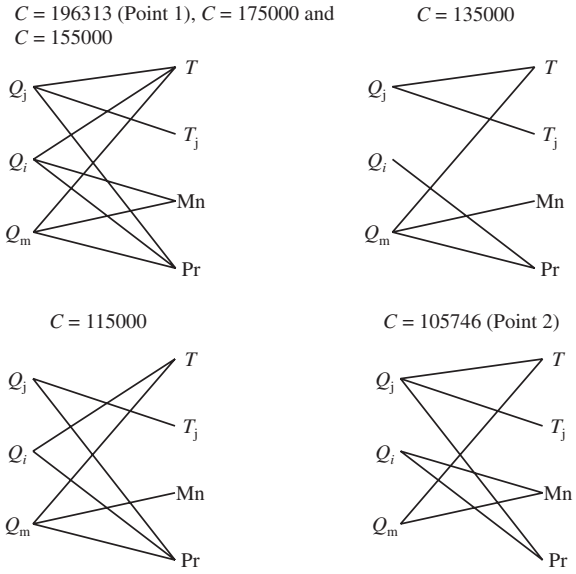

Fig. 7. Pairings between manipulated and controlled variables corresponding to the optimal designs for the B to A grade transition.

fastest grade transition, to point 2, the lowest cost design. From this set, the preferred solution can be selected according to some additional criteria. It is possible to base this decision on techniques that quantitatively assess the trade-offs between the different Pareto set points (Takeda and Ray, 1999; Luyben and Floudas, 1994), and/or use a qualitative criteria coming from an engineering knowledge of the process.

Fig. 5 shows that the lowest cost design represents a reduction of 46% in capital and steady-state operating costs with respect to the fastest grade transition design. The difference in grade transition speed of the optimal designs of the Pareto set is better appreciated in Fig. 6, which shows the optimal time trajectory of the polymer *Mn* corresponding to each of the Pareto set points. It is possible to observe that with point 2 design, grade A specification is reached approximately 10 min later than with point 1 design, which means an increase of 25% in transition time. The *Mn* profiles corresponding to the intermediate designs are shown in Fig. 6 with dotted lines. It should be noted that, in all cases, the optimally designed control system allows reaching the target *Mn* with minimal overshoot, and a strict matching with the desired value of this property afterwards. Polydispersity profiles showed a similar trajectory than the one of the A to B transition in all cases. The optimal pairings of the multivariable PI controllers of each control system design are shown in Fig. 7. In general, these pairings were different for each control system design.

It is important to note that all the optimal designs represented in Fig. 5 include the smallest reactor and the initiator AIBN, which coincides with the optimal design of the A to B transition. The steady states corresponding to the optimal designs of the Pareto set for the B to A transition are presented in Table 6. Interestingly, in all cases the operating point for polymer grade A is almost the same as in the A to B transition. However, for the fastest B to A transition design (first row of Table 6), grade B is produced at a lower temperature than in the A to B case. This temperature reduction is compensated with a higher initiator flow rate, which increases the operating costs (see Table 5). Lower cost optimal designs for the B to A case (but presenting a slower grade transition) result from a reduction in grade B operating costs by means of a smaller initiator flow rate. Although the jacket flow rate is increased at the same time, its cost is negligible in comparison with that of the initiator. It is interesting to see how the operating temperature for grade B production is increased while the initiator flow rate is reduced in order to obtain the same *Mn*. As a consequence of the higher temperature, the monomer conversion in grade B operating point is higher in the lower cost designs. Although all conversion levels are acceptable for our design specifications, the higher conversion is another advantage for the low cost designs.

Another feature that arises when analyzing the results in Table 7 is that the polymer with higher *Mn* (grade A) is

Table 6
Optimal steady-states designs corresponding to the different points of the Pareto set of the BA transition

C ($/year^{-1})	Gt	T_A (°C)	T_B (°C)	$T_{j,A}$ (°C)	$T_{j,B}$ (°C)	T_f (°C)	$Q_{i,A}$ (L s^{-1})	$Q_{i,B}$ (L s^{-1})	$Q_{j,A}$ (L s^{-1})	$Q_{j,B}$ (L s^{-1})	x_A	x_B
196 313	10.3×10^{-4}	98	76	53	40	67	2.56×10^{-3}	8.84×10^{-3}	0.079	0.109	0.32	0.18
175 000	10.5×10^{-4}	100	79	54	41	67	2.51×10^{-3}	7.62×10^{-3}	0.080	0.111	0.33	0.20
155 000	10.9×10^{-4}	100	82	54	41	67	2.51×10^{-3}	6.42×10^{-3}	0.080	0.115	0.32	0.22
135 000	11.2×10^{-4}	100	85	54	42	67	2.51×10^{-3}	5.23×10^{-3}	0.080	0.121	0.33	0.25
115 000	11.8×10^{-4}	100	92	54	43	67	2.51×10^{-3}	4.03×10^{-3}	0.080	0.131	0.33	0.31
105 746	12.8×10^{-4}	100	100	54	45	66	2.51×10^{-3}	3.48×10^{-3}	0.079	0.138	0.33	0.37

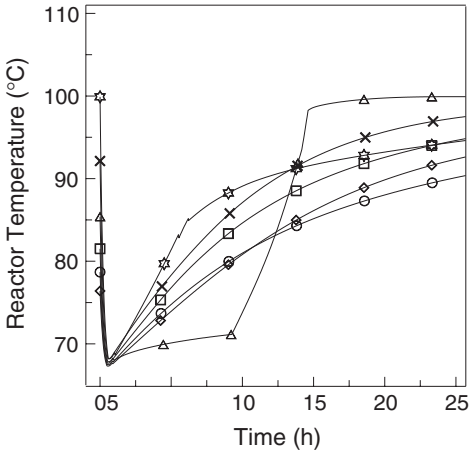

Fig. 8. Reactor temperature profiles corresponding to the optimal designs for the B to A grade transition. ◇— Point 1 ($C = 196\,313$), ○— $C = 175\,000$, □— $C = 155\,000$, △— $C = 135\,000$, ×— $C = 115\,000$, ☆— $C = 105\,746$.

produced at a higher temperature. A priori, it would be expected that if steady-state operating temperature increases molecular weight decreases due to faster generation of initiator radicals produced by first order initiator decomposition rate. Model results shown in Table 6 do not agree with this prediction. This controversial result is explained by analyzing both operating temperature and initiator flow rate simultaneously. To be able to obtain a higher molecular weight by increasing temperature the reactor must operate at a lower initiator flow rate, as shown in Table 6. To keep temperature at a desired level at low initiator flow rate, while restricting jacket inlet temperature to be the same in both stead-states, the jacket fluid flow rate decreases with respect to the one obtained for grade B production.

Fig. 8 depicts the temperature profiles corresponding to the dynamic simulations of the optimal designs. It is interesting to note that all temperature profiles, starting from the different steady-state temperatures of grade B production, show a similar initial steep descent to approximately 68 °C, followed by a comparatively slow rise to the steady-state temperature of grade A production, which is in all cases around 100 °C. The time needed to reach the minimum temperature varies from 34 min in the fastest transition designs, to 40 min in the slowest transition design. This value corresponds to the time needed to perform approximately 95% of the total change in the polymer *Mn*. Monomer concentration initially shows a steep increase followed by a slow decrease to the steady-state value, while the initiator behaves in the opposite way. It should be noted that temperature, monomer concentration and initiator concentration profiles present opposite tendencies to their counterparts of the A to B transition.

It is important to point out that the transition time needed for a grade transition is strongly dependent on the direction of the change in the polymer property. For the particular system studied in this work, transition from grade B to grade A always required more time than the opposite transition. Notice from Figs. 6 and 3, that even the fastest B to A transition in the optimal Pareto set for this transition (Fig. 6), is more than twice as slow as the A to B transition (Fig. 3). This kind of behavior has also been observed in studies on optimal grade transition for other systems (Chatzidoukas et al., 2003).

5.3. Cyclic transitions between grades A and B

Results shown up to this point showed that when A to B and B to A transitions are considered separately, the optimal operating point for grade B production might be different according to the direction of the transition. However, this is not acceptable if the plant is meant to perform A to B and back to A sequential transitions. This is why, in order to obtain an optimal design capable of performing sequential transitions between grades A and B, both transitions were considered simultaneously in the dynamic simulation as explained before. In this way, a single set of process design variables is obtained (reactor unit, initiator type, and grade A and B operating points). However, the control system (feedforward signals, pairings between controlled and manipulated variables, and controller tuning parameters) can vary depending on the direction of the transition.

The solution of the multiobjective MIDO yielded a Pareto set that coincides with that of the B to A transition case (see Fig. 5) except for a displacement of $+3.5 \times 10^{-4}$ in the *Gt*-axis. Following the notation used in the B to A transition design, in what follows point 1 design will stand for the Pareto set point that results in the best grade transition, and point 2 in the one that presents the lowest cost. The mentioned displacement may be related to the existence of only one *Gt* in the Pareto set for the single A to B transition case ($Gt = 3.5 \times 10^{-4}$), which coincides with the transition time obtained for all the A to B transition in the cyclic case. We should now explain the coincidence between the *Gt* for the single B to A transition and the

Table 7
Optimal steady-states designs corresponding to the different points of the Pareto set of the ABA transition

C	Gt		T_A	T_B	$T_{j,A}$	$T_{j,B}$	T_f	$Q_{i,A}$	$Q_{i,B}$	$Q_{j,A}$	$Q_{j,B}$	x_A	x_B
($/year^{-1})	B to A	A to B	(°C)	(°C)	(°C)	(°C)	(°C)	(L s^{-1})	(L s^{-1})	(L s^{-1})	(L s^{-1})		
195 457	10.3×10^{-4}	3.5×10^{-4}	100	76	54	40	67	2.51×10^{-3}	8.84×10^{-3}	0.080	0.109	0.33	0.18
175 000	10.5×10^{-4}	3.5×10^{-4}	100	79	54	41	67	2.51×10^{-3}	7.62×10^{-3}	0.080	0.111	0.33	0.20
155 000	10.9×10^{-4}	3.5×10^{-4}	100	82	54	41	67	2.51×10^{-3}	6.42×10^{-3}	0.080	0.115	0.32	0.22
135 000	11.2×10^{-4}	3.5×10^{-4}	100	85	54	42	67	2.51×10^{-3}	5.23×10^{-3}	0.080	0.121	0.33	0.25
115 000	11.8×10^{-4}	3.5×10^{-4}	100	92	54	43	67	2.51×10^{-3}	4.03×10^{-3}	0.080	0.131	0.33	0.31
105 746	12.8×10^{-4}	3.5×10^{-4}	100	100	54	45	66	2.51×10^{-3}	3.48×10^{-3}	0.079	0.138	0.33	0.37

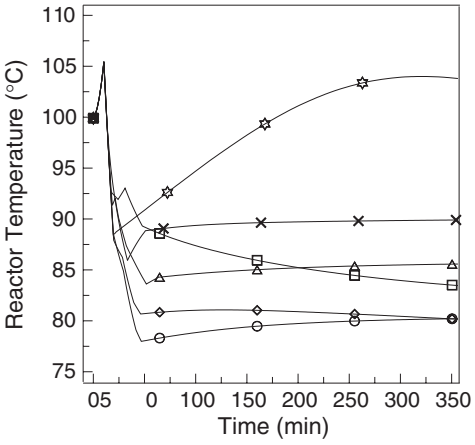

Fig. 9. Reactor temperature profiles during the A to B transition corresponding to the optimal designs for the A to B cyclic transitions. —◇— Point 1 ($C = 195\,457$), —○— $C = 175\,000$, —□— $C = 155\,000$, —△— $C = 135\,000$, —×— $C = 115\,000$, —☆— $C = 105\,746$.

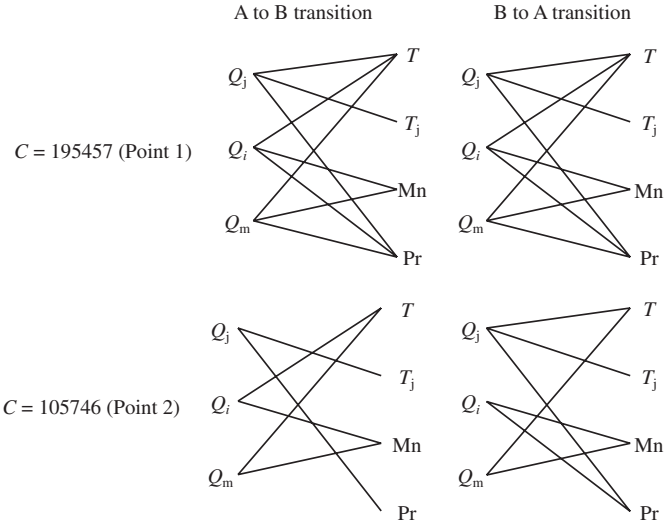

Fig. 10. Pairings between manipulated and controlled variables corresponding to point 1 and point 2 optimal designs for the cyclic transitions between grades A and B. Pairings of the other designs of the Pareto set are the same as those of point 1.

Gt portion corresponding to the B to A transition in the cyclic case. Table 7 shows the optimal process design variables corresponding to this set. As can be seen, the results almost coincide with those of the B to A transition. This indicates that the more time-consuming transition, from B to A, dominates the selection of the optimal process design. In other words, in order to reduce the global transition time for the cyclic transitions, the optimizer selects a design that favors the B to A transition over the opposite one. This is not an unexpected result, since as was shown in the previous sections for single transition operation, the B to A transition took at least as twice as long as the A to B one. The last row of Table 7 coincides with the optimal process design for the A to B transition case (see Table 5); logically, the portion of *Gt* corresponding to the A to B transition in the cyclic case (that measures the best transition between steady states) is the same as in the single AB transition. As noted before, this portion of *Gt* corresponding to the A to B transition is the same for all the different process designs. That is, there are several design alternatives for this transition, which appear to be as good as the one encountered when optimizing the A to B transition only. This was verified by plotting the *Mn* profile resulting from the different optimal process designs. The curves overlapped with that presented in Fig. 3, except for negligible differences after the undershoot zone. In order to explain this behavior we turn to the example in Fig. 9. This figure shows the optimal temperature profiles during the A to B transition between the steady states reported in Table 7. It can be seen that, starting from the 100 °C point that is common to all designs, the trajectories are almost the same in the first 20 min, and then they follow different paths to their corresponding steady-state temperature for grade B production. The same applies to the other process variables. The first 20 min comprise the time needed to take the polymer *Mn* to its target value (see Fig. 3) and yields the most significant contribution to the value of the objective function *Gt*, because *Mn* is kept very near the target value thereon. In other words, equivalent alternatives for the grade B operating point exist for the A to B transition because, after a common initial trajectory where *Mn* is driven to the desired value, the optimal control systems can take the process to the different steady states for grade B production while keeping *Mn* at its set point at the same time. In the first case analyzed, the A to B transition, the optimizer found one of these almost equivalent designs.

The control structures for the optimal designs of the Pareto set are shown in Fig. 10. It can be noticed that, for the B to A transition, the variable pairings in two of the optimal designs in the cyclic transition case (those corresponding to $C = 135\,000$

and $C = 115\,000$) did not coincide with the ones obtained in the B to A (single transition) case, although the process designs and the values of *Gt* are almost the same (see Tables 6 and 7). That is, for the same process designs the optimizer now found, in some of the solutions, different control systems that allowed obtaining the same time trajectory for the polymer *Mn*. For the other process variables, the trajectories until the grade A *Mn* was achieved were the same, although then different routes might be followed until the same final steady state was reached.

The time needed to solve the MIDO problems for the different points of the Pareto set varied between 3 and 12 h in a Pentium IV 2.8 GHz CPU, depending on the number of MILP iterations and the time required for each of the dynamic optimization subproblems. This was also the case for the previous two cases analyzed.

6. Conclusions

In this work the simultaneous design and control of a solution styrene polymerization process was performed using a multiobjective mixed-integer dynamic optimization approach. Design objectives comprised minimization of off-specification polymer and transition time during grade changeover between two polystyrene grades. Capital and steady-state operating costs were also minimized.

The simultaneous approach allowed to obtain designs that minimize the objective functions and also guarantee controllability during operation for the considered scenarios. The strong interaction between process design and control has been contemplated with this methodology.

Optimal steady-state operating points varied with the direction of the transition. If the process is meant to perform a single transition from grade A (the higher molecular weight polymer) to grade B (the lower molecular weight polymer), there was not any compromise between objectives and a single optimum, rather than a Pareto set, was found. For the opposite situation, a single transition from grade B to grade A, a Pareto set was obtained. Grade B polymer is produced at lower temperatures for optimal transition, and at higher temperatures for minimizing operating costs. The optimal operating point for the other grade was approximately the same in all cases.

The optimal transition from grade B to grade A requires more time and originates more off-specification material than the optimal transition in the opposite direction. Therefore, when the system was designed to perform changeovers in the two directions, transition from B to A dominated and the optimal process designs from this Pareto set almost coincided with the ones obtained for the single transition from grade B to A. However, this did not affect transition from A to B, since this grade change is mostly influenced by grade A operating point, which remained unchanged.

In all cases, optimal process designs included the smallest reactor and initiator AIBN, which means that these are the best choices to minimize costs and to optimize grade transition. Although the first decision is consistent with capital cost reduction and fast dynamics, the selected initiator was the most expensive of the possible alternatives. Evidently, the decomposition properties of this initiator allow smaller flow rates resulting in lower operating costs.

Each one of the optimal process designs was obtained together with an optimal control system. In all cases, the control systems allowed a grade transition with minimum undershoot and off-specification product. Besides, process constraints during transition were always satisfied.

In the two cases where a Pareto set was obtained, simple inspection of the Pareto points based on an engineering knowledge of the process was enough guide for the selection of the final design. Since transition time is much lower than reactor residence time for all the optimal points of the Pareto sets, an increase in this time can be afforded in view of the high reduction in capital and steady-state costs accompanied with higher steady-state conversions. Therefore, the lower costs designs of the Pareto sets turned out to be the best options.

Forthcoming work will address multiple grade transition sequences and other polymer grade specifications.

Notation

a	parameter of the operating costs functions
$A_{d,\mathrm{AIBN}}$	pre-exponential factor of the decomposition constant of initiator AIBN
$A_{d,\mathrm{TBPB}}$	pre-exponential factor of the decomposition constant of initiator TBPB
A_p	pre-exponential factor of the propagation constant
A_{tc}	pre-exponential factor of the termination by combination constant
AIBN	azobis(isobutyronitrile)
c_1	cost parameter
c_2	cost parameter
c_3	cost parameter
C	objective function that comprises capital and steady-state operating costs
C_{cool}	coolant cost
C_{in}	initiator cost
$C_{\mathrm{op,A}}$	operating costs at grade A steady state
$C_{\mathrm{op,B}}$	operating costs at grade B steady state
C_R	reactor cost
Cp	reacting mixture heat capacity
Cp_j	coolant heat capacity
d	discrete variable (reactor volume)
D	set of three discrete variables representing allowed reactor volumes
effic	initiator decomposition efficiency
$E_{d,\mathrm{AIBN}}$	activation energy of the decomposition constant of initiator AIBN
$E_{d,\mathrm{TBPB}}$	activation energy of the decomposition constant of initiator TBPB
E_p	activation energy of the propagation constant
E_{tc}	activation energy of the termination by combination constant
g_e	set of end-point inequalities
g_q	set of time invariant inequalities

Gt	objective function for grade transition optimization
h_0	set of initial conditions
h_a	set of algebraic equations
h_d	set of differential equations
h_y	set of pure integer equalities
I	molar initiator concentration
I_{f0}	nominal value of the initiator concentration in the feed stream
k_{dI}	kinetic constant for initiator decomposition
k_{dM}	kinetic constant for monomer thermal decomposition
k_p	kinetic constant for propagation reaction
k_{tc}	kinetic constant for termination reaction
$K_{i,j}$	controller gain of the PI loop between the *ith* manipulated variable and the *jth* controlled variable
$K_{i,j}^{lb}$	lower bound for the controller gain $K_{i,j}$
$K_{i,j}^{ub}$	upper bound for the controller gain $K_{i,j}$
M	molar monomer concentration
M_0	zeroth order moment of the polymer chain length distribution
M_1	first order moment of the polymer chain length distribution
M_2	second order moment of the polymer chain length distribution
M_{f0}	nominal value of the monomer concentration in the feed stream
Mn	number average molecular weight
Mn_{A}	number average molecular weight of grade A polymer
Mn_{B}	number average molecular weight of grade B polymer
Mn_{AB}	number average molecular weight when performing the transition from grade A to B in the cyclic transitions case
Mn_{BA}	number average molecular weight when performing the transition from grade B to A in the cyclic transitions case
Mn_{Target}	target value of the Mn during grade transition
Mw	weight average molecular weight
Mw_{AIBN}	molecular weight of the initiator AIBN
Mw_{M}	monomer molecular weight
Mw_{TBPB}	molecular weight of the initiator TBPB
p	set of model parameters
Pd	polydispersity
Pr	polymerization rate
Q	total flow rate (sum of the feed streams)
Q_0	nominal value of the total flow rate
Q_i	initiator flow rate
Q_i^*	overall control action over the initiator flow rate
Q_j	coolant flow rate
Q_j^*	overall control action over the coolant flow rate
Q_m	monomer flowrate
Q_m^*	overall control action over the monomer flow rate
Q_s	solvent flow rate
$R1$, $R2$ and $R3$	options for the reactor unit
t	time
t_f	time horizon
T	reactor temperature
T_{f0}	nominal value of the feed stream temperature
T_j	jacket temperature
TBPB	*tert*-butyl peroxybenzoate
u^{lb}	set of lower bounds on the time-varying optimization variables
u^{ub}	set of upper bounds on the time-varying optimization variables
$u(t)$	set of time-varying optimization variables
U_i	*i*th manipulated variable
U_i^*	overall control action over the *i*th manipulated variable
$U_{i,\mathrm{ff}}$	feedforward signal for the *i*th manipulated variable
$U_{i,\max}$	upper limit for the *i*th manipulated variable
$U_{i,\min}$	lower limit for the *i*th manipulated variable
UA	heat-transfer parameter
UA_0	nominal value of the parameter UA
V	reactor volume
V_0	nominal value of the reactor volume
V_j	jacket volume
x	monomer conversion
x_a	set of time-varying algebraic variables
x_a^*	set of time invariant algebraic variables
$x_d(t)$	differential state variables
$\dot{x}_d(t)$	set of time derivatives of the differential state variables
y	set of binary variables
y_{AIBN}	binary variable associated with the selection of the initiator AIBN
Y_j	*j*th controlled variable
$Y_{j,\mathrm{set}}$	set point of the *j*th controlled variable
y_{TBPB}	binary variable associated with the selection of the initiator TBPB
z	set of time invariant optimization variables
z^{lb}	setof lower bounds on the time invariant optimization variables
z^{ub}	set of upper bounds on the time invariant optimization variables

Greek letters

$\Delta \mathrm{H}_r$	reaction enthalpy
ε	parameter of the ε-constraint method
$\varepsilon_{\max}$	maximum value of parameter ε
$\varepsilon_{\min}$	minimum value of parameter ε
ζ	model parameter
λ_0	global radical concentration
ρ	reacting mixture density
ρ_j	coolant density

$1/\tau_{i,j}$ reset rate of the PI loop between the *ith* manipulated variable and the *jth* controlled variable

Subscripts

f feed conditions
A grade A steady state
B grade B steady state

Superscripts

$\bar{\cdot}$ dimensionless variable

Acknowledgments

The authors thank UNS, CONICET and ANPCyT for their financial support.

References

Asteasuain, M., Ugrin, P.E., Lacunza, M.H., Brandolin, A., 2001. Effect of multiple monomer feedings in the operation of a high pressure polymerization reactor for ethylene polymerization. Polymer Reaction Engineering 9 (3), 163–182.

Asteasuain, M., Brandolin, A., Sarmoria, C., 2003. Molecular weight distributions in styrene polymerization with asymmetric bifunctional initiators. Polymer 45, 321–335.

Bahri, P., Bandoni, A., Romagnoli, J., 1997. Integrated flexibility and controllability analysis in design of chemical processes. A.I.Ch.E. Journal 43, 997–1015.

Bansal, V., Perkins, J.D., Pistikopoulos, E.N., 2002. A case study in simultaneous design and control using rigorous, mixed-integer dynamic optimization models. Industrial and Engineering Chemical Research 41, 760–778.

BenAmor, S., Doyle III, F.J., McFarlane, R., 2004. Polymer grade transition control using advanced real-time optimization software. Journal of Process Control 14, 349–364.

Bindlish, R., Rawlings, J.B., 2003. Target linearization and model predictive control of polymerization processes. A.I.Ch.E. Journal 49 (11), 2885–2899.

Bhaskar, V., Gupta, S.K., Ray, A.K., 2000. Applications of multiobjective optimization in chemical engineering. Reviews in Chemical Engineering 16 (1), 1–54.

Bhat, S.A., Sharma, R., Gupta, S.K., 2004. Simulation and optimization of the continuous tower process for styrene polymerization. Journal of Applied Polymer Science 94 (2), 775–788.

Brandolin, A., Vallés, E.M., Farber, J.N., 1991. High pressure tubular reactors for ethylene polymerization, optimization aspects. Polymer Engineering and Science 31, 381–390.

Cervantes, A.M., Tonelli, S., Brandolin, A., Bandoni, J.A., Biegler, L.T., 2002. Large-scale dynamic optimization for grade transition in a low density polyethylene plant. Computers and Chemical Engineering 26, 227–237.

Chatzidoukas, C., Perkins, J.D., Pistikopoulos, E.N., Kiparissides, C., 2003. Optimal grade transition and selection of closed-loop controllers in a gas-phase olefin polymerization fluidized bed reactor. Chemical Engineering and Science 58, 3643–3658.

Choi, K.Y., 1986. Analysis of steady state of free radical solution polymerization in a continuous stirred tank reactor. Polymer Engineering and Science 26, 975–981.

Costa Jr., E.F., Lage, P.L.C., Biscaia Jr., E.C., 2003. On the numerical solution and optimization of styrene polymerization in tubular reactors. Computers and Chemical Engineering 27, 1591–1604.

Douglas, J.M., 1985. A hierarchical decision procedure for process synthesis. A.I.Ch.E. Journal 31, 353–362.

Ellis, M.F., Taylor, T.W., Jensen, K.F., 1994. On-line molecular weight distribution estimation and control in batch polymerization. A.I.Ch.E. Journal 40 (3), 445–462.

Embiruçu, M., Lima, E.L., Pinto, J.C., 1996. A survey of advanced control of polymerization reactors. Polymer Engineering and Science 36 (4), 433–447.

Fontoura, J.M.R., Santos, A.F., Silva, F.M., Lenzi, M.K., Lima, E.L., Pinto, J.C., 2003. Monitoring and control of styrene solution polymerization using NIR spectroscopy. Journal of Applied Polymer Science 90, 1273–1289.

Guria, C., Verma, M., Mehrotra, S.P., Gupta, S.K., 2005. Multi-objective optimal synthesis and design of froth flotation circuits for mineral processing using the jumping gene adaptation of genetic algorithm. Industrial and Engineering Chemistry Research 44, 2621–2633.

Hidalgo, P.M., Brosilow, C.B., 1990. Nonlinear model predictive control of styrene polymerization at unstable operating points. Computers and Chemical Engineering 14 (4/5), 481–494.

Kim, K.J., 1991. Modeling and control of continuous free radical polymerization reactors. Ph.D. Thesis, Department of Chemical Engineering, University of Maryland, College Park, MD.

Kookos, I.K., Perkins, J.D., 2001. An algorithm for simultaneous process design and control. Industrial and Engineering Chemistry Research 40, 4079–4088.

Luyben, M.L., Floudas, C.A., 1994. Analyzing the interaction of design and control—1. A multiobjective framework and application to binary distillation synthesis. Computers and Chemical Engineering 18 (10), 933–969.

Matches, 2004. ⟨www.matche.com/EquipCost/Reactor.htm⟩.

McAuley, K.B., MacGregor, J.F., 1992. Optimal grade transitions in a gas phase polyethylene reactor. A.I.Ch.E. Journal 38, 1564–1576.

McKenna, T.F., 1996. Computer aided process design: short-cut design for polymer production. Computers and Chemical Engineering 20, S237–S242.

McKenna, T.F., Malone, M.F., 1990. Polymer process design. I. Continuous production of chain growth homopolymers. Computers and Chemical Engineering 14 (10), 1127–1149.

Na, S., Rhee, H., 2002. An experimental study for property control in a continuous styrene polymerization reactor using a polynomial ARMA model. Chemical Engineering and Science 57, 1165–1173.

Nascimento, C.A.L., Giudici, R., Guardani, R., 2000. Neural network based approach for optimization of industrial chemical processes. Computers and Chemical Engineering 24, 2303–2314.

Ponnuswamy, S.R., Shah, S.L., Kiparissides, C.A., 1987. Computer optimal control of batch polymerization reactors. Industrial and Engineering Chemistry Research 26, 2229–2236.

Prasad, V., Schley, M., Russo, L.P., Bequette, B.W., 2002. Product property and production rate control of styrene polymerization. Journal of Process Control 12 (3), 353–372.

Process Systems Enterprise, Ltd., 2005. gPROMS introductory user guide.

Ray, A.K., Gupta, S.K., 1985. Optimization of nonvaporizing nylon 6 reactors with stopping conditions. Journal of Applied Polymer Science 30, 4529–4550.

Ray, A.K., Gupta, S.K., 1986. Optimization of nonvaporizing nylon 6 reactors with stopping conditions and end-point constraints. Polymer Engineering and Science 26, 1033–1044.

Russo, L.P., Bequette, B.W., 1998. Operability of chemical reactors: multipliciy behaviour of a jacketed styrene polymerization reactor. Chemical Engineering Science 53 (1), 27–45.

Schweiger, C.A., Floudas, C.A., 1997. Interaction of design and control: optimization with dynamic models. In: Hager, W.W., Pardalos, P.M. (Eds.), Optimal Control: Theory, Algorithms and Applications, Kluwer Academic BV, Dordrecht, p. 388.

Simon, R.H.M., Chappelear, D.C., 1979. Technology of styrenic polymerization reactors and processes. In: Gould, R.F. (Ed.), Polymerization Reactors and Processes, ACS Symposium Series, vol. 104, American Chemical Society, Washington, DC, p. 71.

Srivastava, D., Gupta, S.K., 1991. Optimization of a tubular nylon 6 reactor with radial gradients. Polymer Engineering and Science 31, 596–606.

Stepto, K., Horie, K., Kitayama, T., Abe, A., 2003. Mission and challenges of polymer science and technology. Pure Applied Chemistry 75 (10), 1359–1369.

Takeda, M., Ray, W.H., 1999. Optimal grade transition strategies for multistage polyolefin reactors. A.I.Ch.E. Journal 45, 1776–1793.

Tsoukas, A., Tirrel, M., Stephanopoulos, G., 1982. Multiobjective dynamic optimization of semibatch copolymerization reactors. Chemical Engineering and Science 37 (12), 1785–1795.

United States Patent 4,376,847, Mitsui Toatsu Chemicals, Inc. (Tokyo, JP), 1981.

United States Patent: 5,191,040, Idemitsu Petrochemical Co., Ltd. (Tokyo, JP), 1992.

United States Patent: 5,455,321, The Dow Chemical Company (Midland, MI), 1994.

Wang, H.F., 2003. Interactions and multivariable design of STATCOM AC and DC voltage control. Electrical Power and Energy Systems 25, 387–394.

Wang, Y., Seki, H., Ohyama, S., Akamatsu, K., Ogawa, M., Ohshima, M., 2000. Optimal grade transition control for polymerization reactors. Computers and Chemical Engineering 24, 1555–1561.

Yi, H., Kim, J.H., Han, C., Lee, J., Na, S., 2003. Plantwide optimal grade transition for an industrial high-density polyethylene plant. Industrial and. Engineering Chemistry Research 42, 91–98.